Space-borne global astrometric surveys: the hunt for extra-solar planets.

M.G. Lattanzi,[1] A. Spagna,[1] A. Sozzetti,[1,2] S. Casertano,[2]⋆

[1] *Osservatorio Astronomico di Torino, Pino Torinese TO, I-10025, Italy*
[2] *Space Telescope Science Institute, Baltimore MD, 21218, USA*

ABSTRACT

The proposed global astrometry mission *GAIA*, recently recommended within the context of ESA's Horizon 2000 Plus long-term scientific program, appears capable of surveying the solar neighborhood within ~ 200 pc for the astrometric signatures of planets around stars down to the magnitude limit of V=17 mag, which includes late M dwarfs at 100 pc.

Realistic end-to-end simulations of the GAIA global astrometric measurements have yielded first quantitative estimates of the sensitivity to planetary perturbations and of the ability to measure their orbital parameters. Single Jupiter-mass planets around normal solar-type stars appear detectable up to 150 pc ($V \leqslant 12$ mag) with probabilities $\geqslant 50$ per cent for orbital periods between ~ 2.5 and ~ 8 years, and their orbital parameters measured with better than 30 per cent accuracy to about 100 pc. Jupiter-like objects (same mass and period as our giant planet) are found with similar probabilities up to 100 pc.

These first experiments indicate that the *GAIA* results would constitute an important addition to those which will come from the other ongoing and planned planet-search programs. These data combined would provide a formidable testing ground on which to confront theories of planetary formation and evolution.

Key words:
astrometry – stars:planetary systems – artificial satellites,space probes

1 INTRODUCTION

At the very end of 1995, the discovery (Mayor & Queloz 1995) of the first Jupiter-mass (M_J) planet orbiting a normal star other than the Sun heralded the beginning of a new era of extraordinary discoveries in the realm of extra-solar planets, bringing with them the hope for a better understanding of the formation and frequency of planetary systems, and perhaps of bringing us closer to the ultimate goal of discovering extraterrestrial life.

After four years since that discovery, spectroscopic programs have been able to reveal some twenty extra-solar planets, i.e., objects with a lower mass limit below the 13-M_J cut-off which has been adopted by Oppenheimer and Kulkarni (1999) to differentiate giant planets from brown dwarfs.

However, these discoveries have raised new and troubling questions in our understanding of the properties of planetary systems. The fundamental tenets upon which present theories are based include nearly circular orbits

and giant planets formed several AU from the central star, in contrast with the very short orbital periods (Mayor & Queloz 1995) and high eccentricities (Latham et al. 1989; Cochran et al. 1996; Mazeh et al. 1996) found for several of the new discoveries. Their interpretation as *bona-fide* planets rests on our understanding of correlations shown by their orbital and physical parameters, as recently discussed by Black (1997) and earlier by Duquennoy & Mayor (1991) in their work on solar-type binary stars.

New models, which employ specific physical and dynamical mechanisms like *in-situ* formation (Bodenheimer et al. 1999) or orbital migration (Lin et al. 1996; Trilling et al. 1998; Murray et al. 1998), have been proposed to justify the presence of *hot jupiters* around normal stars, demonstrating that the interplay between additional theoretical work and more observational data will be necessary for a continued improvement in our theoretical understanding of how planets form and evolve, and where Earth-like planets could eventually be found.

However, simply adding a few tens of additional detections of giant extra-solar planets is not enough. A better un-

derstanding of the conditions under which planetary systems form and of their general properties requires large, *complete* samples of planets, with useful upper limits on Jupiter-mass planets at several AU from the central star.

Ongoing and planned radial velocity surveys (Mayor & Queloz 1995; Cochran et al. 1996; Noyes et al. 1997; Marcy & Butler 1992; Marcy & Butler 1998) have started filling significant portions of the relevant parameter space. Searches based on relative astrometry from the ground and in space (Gatewood 1987; Colavita et al. 1999; Colavita et al. 1998; Mariotti et al. 1998; Pravdo & Shaklan 1996) will be an important complement to the spectroscopic work and, probably, the preferred means for establishing the existence of planets around young stars and that of low mass planets down to a few Earth masses, as will be the case for SIM (Boden et al. 1997; Unwin 1999).

A *HIPPARCOS*-like, space-borne global astrometric mission, which can survey the whole sky to faint magnitudes and with high astrometric accuracy, will enable the monitoring of large ($> 10^5$) samples of stars, with well understood completeness properties. This, depending on actual values of planetary frequencies (Marcy et al. 1999), could yield the possibility of making firm measurements of statistical properties of planetary systems. For, different correlations among orbital parameters (eccentricity, period or semi-major axis) and measurable differences in planetary frequency are likely to be generated by diverse planetary formation scenarios (core accretion and disk instability are the two known to date) and evolution mechanisms, as well as different formation and evolution processes of the parent star (binarity, spectral type, metallicity, age). An astrometric mission such as *GAIA* appears well poised for such a systematic census of planetary systems within ~ 200 pc from the Sun.

The *GAIA* concept was originally proposed by Lindegren and Perryman (1996) as a possible Cornerstone–class mission within the Horizon 2000+ program of scientific satellites of the European Space Agency. This satellite is designed to chart more than one billion objects (stars, extra-galactic objects, and solar system objects) on the sky down to the limiting magnitude of $I = 20$. The targeted final accuracy is ~ 10 μas on positions and parallaxes, and ~ 10 μas/year on proper motions at the reference magnitude of $V = 15$ for a G2V star (Gilmore et al. 1998), and for a mission life time of 5 years.

In the following sections we show and discuss some relevant results derived from detailed end-to-end simulations of the data acquisition and analysis process for *GAIA*, which, as we will see, appears capable of discovering Jupiter-mass planets around $\sim 3 \times 10^5$ candidate stars (including dwarfs earlier than K5).

2   DATA SIMULATION

The simulation code is an adaptation of that used by Galligani et al. (1989) for the assessment of the astrometric accuracy of the sphere reconstruction in the *HIPPARCOS* mission. We generate catalogs of single stars randomly distributed on the sky; each run produces a sphere of 200 stars. As the satellite observing strategy (or scanning law) is most easily described in ecliptic coordinates, positions, proper motions and parallax (λ, β, μ_λ, μ_β, and π, respectively)

are also given in the same coordinate system. For the moment, μ_λ, μ_β and π, as well as magnitudes and colors, are drawn from simple distributions which do not represent any specific Galaxy model; in particular, in each run the 200 stars simulated have the *same* parallax, total proper motions, magnitudes, and colors.

The satellite is made to sweep the sky in such a way that the spin axis precesses around the Sun at a rate of about 6.5 rev/year and with a constant angle of 43 deg. Stars that at any given time are "seen" within a strip ~ 1 deg wide along the great circle (GC) being scanned are considered observed; a GC is completed in about 2.5 hours. Basic observations, which in principle can easily be derived from the fringe pattern measurements above, are the abscissae along a GC, as *GAIA*, like *HIPPARCOS*, makes very precise measurements in one dimension only. The mission lifetime is set to 5 years and the scanning law is such that the number of basic observations per star is a function of ecliptic latitude: each given object on the sky is re-observed approximately every month, for a total of ~ 60 one-dimensional position measurements, on average. The minimum number of observations is ~ 30 and occurs for stars at the ecliptic equator. The position of a star at a given time, as described by the combined effects of parallax and proper motions, is called here *barycentric* location and it has been described in Euclidean space (flat Lorentzian). General relativistic effects, which will have to be considered in the future (especially for the case of Earth-like planets), are not taken into account.

Finally, gravitational perturbations (Keplerian motions) induced by a (*single*) nearby orbiting mass are added to the barycentric location resulting in the "true" *geometric* location of a target.

Simulated observations are generated by adding the appropriate astrometric noise to the true locations. The error sources considered in the simulation are discussed below.

As in *HIPPARCOS*, *GAIA* will have two viewing directions separated by a large angle named Base Angle (BA). It is by connecting directions far apart on the sky that the principle of space-borne global astrometry demonstrated by *HIPPARCOS* is implemented. Therefore, it is not surprising that the accuracy with which the BA is known throughout the mission is probably the most important single item within the *GAIA* concept. At the moment there are two mature optical designs for the BA. One configuration feature two telescopes mounted on the same optical bench and pointing along the two different line-of-sights. The other design uses a beam combiner (an adaptation of that used on *HIPPARCOS*) which physically materializes the BA and multiplexes the two viewing directions into a single telescope unit; beam combiner and telescope are bolted to the same bench. The twin telescopes designed for the first configuration feature an off-axis monolithic primary (with no central obscuration), while the collecting telescope of the latter design is a Fizeau interferometer with a baseline of 2.45m.

The details of the *GAIA* optical configuration (see e.g. Gilmore et al. (1998), and references therein) are not critical to our discussion of photon-driven astrometric errors. The major difference with our earlier work (Casertano et al. 1995) is that both designs feature a significantly increased telescope aperture. The monolithic configuration has a rectangular primary of 1.7m by 0.7m, and each circular aperture of the interferometric option is 0.65m in diameter. High-

Table 1. *Photon and total error for a single observation. This is the combination of $\simeq 8$ consecutive field-of-view crossings, for any given direction on the sky, each comprising 20 elementary 1-sec exposures, for a total duration for the single integration of $\simeq$ 160 sec. These values strictly apply to the interferometric option discussed in the text and to a G2V star and negligible interstellar absorption (Av = 0). The pure photon noise values increase by $\sim$ 30 % for an A0V star and improve by $\sim$ 20 % for a K3V. More explanations are provided in Sections 2.2-2.3*

V mag	Photon error	Total error σ_ψ (μas)	
	(μas)	($\sigma_{\rm b} = 30$ pm)	($\sigma_{\rm b} = 10$ pm)
10	2.4	10.2	3.8
12	5.9	11.5	6.6
15	24.6	26.5	24.8
17	70.3	71.0	70.4
18	129.9	130.3	129.9

accuracy measurements of the position (phase) of the PSFs are made directly on the focal plane using CCD detectors (see next section).

2.1 Payload configurations

The payload design has greatly advanced since the idea sketched in Lindegren & Perryman (1996) and further developed in Loiseau & Shaklan (1996). The two industrial studies commissioned by ESA have looked into the feasibility of two different options for the *GAIA* payload (Gilmore et al. 1998): an all-passive configuration with two identical telescopes (with rectangular-shape monolithic primary mirrors) to be operated in L2, and an all-active configuration with an interferometric (diluted) beam combiner and a Fizeau interferometer as light collector behind it to be operated in geosynchronous orbit. Stability of the BA is passively maintained in the case of the monolithic configuration by utilizing a sophisticated active thermal control system (which must operate at the μK level) and a silicon carbide structure for the optical bench. On the other hand, the interferometric configuration is all-active, with the stability achieved by real-time monitoring implemented via high-accuracy laser metrology (Gai et al. 1997) and control of all critical degrees of freedom.

As we are more familiar with the interferometric option for *GAIA* (Lattanzi et al. 1997), we will be referring to that in the discussion below. However, precision and accuracy requirements and estimates are quite similar for both configurations, especially at the bright magnitudes we are concerned with in this paper.

2.2 Photon noise and point spread function measurement

The ability to measure accurately the position of a star ultimately depends on the width and shape of the point spread function (PSF) of the imaging system and on the number N of photons detected. For a well-sampled PSF, the theoretical limit is shown by (Lindegren 1978) to be $\epsilon = \lambda/(4\pi x_{\rm rms}\sqrt{N})$, where $x_{\rm rms}$ is the rms size of the aperture in the measurement direction. For two circular apertures of diameter D and with a central separation B, we have $x_{\rm rms} = \sqrt{(B/2)^2 + (D/4)^2}$; for the baseline *GAIA* parameters ($B = 2.45$ m, $D = 0.65$ m), $x_{\rm rms} = 1.24$ m (Lin-

degren & Perryman 1995). For $\lambda = 750$ nm (the baselined operational wavelength), this translates into a theoretical monochromatic measurement accuracy of $10\,{\rm mas}/\sqrt{N}$.

The measurement accuracy is degraded for non-monochromatic measurements, by about a factor 2 for a Gaussian filter centered at 7500 Å and 2000 Å wide (Gai et al. 1998). In addition, the requirement of optimal sampling may be difficult to achieve, since the central fringe is only about 0″.04 wide and the field of view is 1 deg. In practice, this will probably cause a loss of accuracy of about 20–40 per cent (Gai et al. 1995; Gai et al. 1998). In the following, we assume a "best reasonable" single-measurement photon noise error of $24\,{\rm mas}/\sqrt{N}$.

Since scans overlap partially, each "observation" of a star will consist of about 8 consecutive scans with 20 sec of integration time allocated per scan, a total integration time of 160 s. Assuming a total collecting area of 0.664 m^2 (2 apertures of 0.65 m diameter) and a total system efficiency of 20 per cent, a star with $V = 15$ would generate about 10^6 photons per observation, corresponding to a photon-limited measurement accuracy of the fringe position of 24 μas. The accuracy scales with the inverse square root of the flux. This approximate calculation agrees with the values in Table 1, obtained for the current version of the interferometric option. The photon noise values (second column in Table 1) for $10 \leqslant V \leqslant 18$ stars were obtained with 3.1 pixels per fringe period, a RON of 3 electrons/pixels, and a DQE of 0.6. Objects brighter than $V = 10$ mag will be also observed by *GAIA*. However, limitations on the dynamic range achievable with CCDs, requires to limit the exposure time for the brighter stars. Thus is practice, the precision starts to level off brighter than $V \simeq 10$.

This accuracy is based on the photon statistics only, and does not take into account possible systematic effects, such as distortions in the optical system or in the detector, imperfection in the fringes, and so on. Many such systematic effects can be calibrated using closure methods, others will require enhancements in system design.

2.3 Accuracy of the Base Angle

The systematic effects mentioned above will lead to residual (systematic) errors in the knowledge of the BA which do not scale with magnitude. Ultimately, these will be the errors which will limit the maximum accuracy of *GAIA* for bright sources. We combine such residual errors in what is hereafter called *residual bias*, or simply *bias*. In the present error budget we assume that the bias can be described as a stationary stochastic process; therefore the bias contributed at the single-observation level to each object (Table 1) scales, like photon noise precision, with the average number of observations collected over the mission lifetime.

The BA can be measured and monitored accurately over time intervals longer than a full revolution ($\geqslant 3$ hours) by making use of the 2π closure properties of the consecutive scans. This is an especially important feature of *GAIA* whose potential, at the *mas* level, has been beautifully proven by *HIPPARCOS*. However, the bias over shorter time scales need to be controlled by ensuring that the relative positions and shapes of all optical elements of the beam combiner do not vary throughout the observation. The necessary sub-nm accuracy will probably be achieved by a combination

of passive control and of laser metrology. For simplicity, we summarize the overall accuracy (bias) with which the (relative) positions of the mirrors of the beam combiner must be known by a single number, the "baseline error" σ_b. This helps visualize the complex interplay of the beam combiner mirrors (which materialize the two baselines of the interferometric design) with a more familiar bias of the type $B \times \delta$, where B is the baseline and δ the angular uncertainty[†]. This also helps understand the bias contribution in Table 1. For example, if the photon error is subtracted (in quadrature) from the total error for the case with $\sigma_b = 30$ pm, the resulting value, ~ 10 μas, represents the angular bias corresponding to that linear "baseline error". Therefore, the requirement on the metrology is $\simeq 3.8$ times more stringent that one would have guessed from the simple calculation $B \times \delta$, with B=2.45 m and δ=10 μas. This example shows that the baseline bias is driven by the dimension of the single mirrors (D=0.65 m) forming the baseline (B/D$\simeq$3.8) within the beam combination system.

Laser metrology in laboratory settings has already achieved extremely high performances, with relative measurements at the picometer level (Gürsel 1993; Noecker et al. 1993; Noecker 1995; Reasenberg et al. 1995). Such precision has been reached over short (few wavelengths) variations in path length, which are appropriate to the *GAIA* design if a good active thermal control is included.

However, the few pm error quoted refers to the precision and stability of a one-dimensional laser gauge measurement of a single optical path. Maintaining the accuracy of the interferometer baseline is much more complex, first, because the three-dimensional positions of several optical elements may need to be monitored simultaneously, and second, because of the possible differences between the optical path of starlight and of the laser gauge beams. Noecker (1995) lists a number of possible systematic errors for the *POINTS* mission concept. An experiment to demonstrate picometer laser metrology for a three-dimensional system on the *GAIA* scale is underway (Gai et al. 1997). For the moment, it remains difficult to give firm figures for the baseline accuracy that will eventually be achieved. In Table 1, we consider two cases which probably bracket realistic expectations: a more "conservative" accuracy $\sigma_b = 30$ pm, which already appears within reach from the preliminary results available, and an "optimistic" accuracy $\sigma_b = 10$ pm. Notice that these bias values are intended at the level of what is called here the single-observation error. The accuracy levels at the end of the mission will be ~ 3 μas and 1 μas for $\sigma_b = 30$ pm and 10 pm, respectively, if errors in successive passes are uncorrelated, as discussed previously. Notice that, for $\sigma_b = 30$ pm, the astrometric precision begins to level off brighter than $V = 12$.

Finally, it is important to mention that the numbers quoted for the linear bias apply to a 3-dimensional monitoring of the relevant structure. The laser beams will have to monitor the corresponding one-dimensional degrees of free-

dom with significantly better resolution—a factor < 2 for the current design.

3 DETECTION AND ORBIT DETERMINATION METHODS

The magnitude of the gravitational perturbations induced by a planet on the parent star, as seen by an astrometric mission, can be quantified through its *astrometric signature* α defined as:

$$\alpha = \frac{M_p}{M_s} \frac{a_p}{d} \qquad (1)$$

where M_p, M_s are the masses of the planet and star respectively, a_p the semi-major axis of the planetary orbit, d the distance of the system from us. If a_p is in AU and d in parsec, then α is expressed in arcsec.

GAIA's sensitivity to this signal depends of course on the errors σ_ψ of each measurement, with theoretical values listed in Table 1. We have verified through tests with different values of σ_ψ (see section 4.1) that, as could be expected, the detection probability depends on σ_ψ and α only through their ratio, the "astrometric" *signal-to-noise ratio*

$$S/N = \alpha/\sigma_\psi, \qquad (2)$$

so that the results obtained can be straightforwardly rescaled to different measurement errors.

For simplicity, we have thus kept the single-observation error fixed at $\sigma_\psi = 10$ μas throughout our simulations. This is the value expected for relatively bright stars ($V \leqslant 12$ mag, corresponding to the Sun at 200 pc), with a conservative baseline error of 30 pm (see Table 1). Our simulations should thus give realistic estimates of: *a) GAIA*'s detectability horizon of planetary mass companions to solar-type stars in the vicinity of our Sun, and *b)* limits on distance for accurate orbital parameters determination.

The starting point for our two-level statistical investigation is the computation of detection probabilities, which will in principle depend upon 1) mission parameters, 2) noise sources, and 3) orbital elements. The contributions to points 1) and 2) are listed in Section 2. As for point 3), we will express the detection probabilities as function of the period P and the signature α, which we expect to be the major contributors, and generally average over the expected distribution of the other orbital parameters.

3.1 Detection

Our first detection method applies a standard χ^2 test (with the confidence level set to 95 per cent) to the residuals $\psi - \psi_r$, where the ψ are the actual measurements, and the ψ_r are the GC abscissae recomputed after fitting the observations of each star with a single-star model, i.e., solving only for the five astrometric parameters appropriate for a single star (position, parallax, and proper motion). Being χ^2_o the value provided by the null model (no planet), the test fails when $\Pr(\chi^2 \leqslant \chi^2_o) \geqslant 0.95$. In this case the planet is considered *detected*. Note that this method only measures deviations from the single-star model, it makes no assumptions on the nature of the residuals nor does it provide initial guesses for

---

[†] While the main contribution to the baseline error will probably come from the relative position of the beam combiner mirrors, the motions and/or distortions of other optical elements (such as the primary apertures of the Fizeau interferometer) can also generate an effective baseline error.

the computation of the planet's mass and orbital parameters.

We employed the χ^2 test to analyze 160 000 stars uniformly distributed on the sky, perturbed by dark companions inducing astrometric signatures α ranging from 10 to 100 μas, with periods P between 0.5 and 20 years. The remaining orbital elements were distributed randomly in the ranges: $0° \leqslant i \leqslant 90°$, $0 \leqslant e \leqslant 1$, $0 \leqslant \Omega \leqslant 2\pi$, $0 \leqslant \omega \leqslant 2\pi$, $0 \leqslant \tau \leqslant P$. The single observation error was set to $\sigma_\psi = 10$ μas, thus the signal-to-noise ratio varied in the range $1 \leqslant S/N \leqslant 10$. Finally, we repeated the same simulations without planets, to verify the correct behaviour of the test and the choice of the confidence level. As expected the number of *false* detections was $\simeq 5$ per cent.

3.2 Orbital parameters

Once a planet is "detected", the goal is to derive reliable estimates for of its orbital elements and mass. For a complete reconstruction of the orbital geometry, we implemented an analytic model in which the observation residuals $\psi - \psi_r$ are evaluated with a recomputed abscissa of the form:

$$\psi_r = \psi_r(\lambda, \beta, \mu_\lambda, \mu_\beta, \pi, T_1, T_2, T_3, T_4, e, P, \tau) \qquad (3)$$

The 1-d measurement along the scanned GC is thus expressed as function of both the standard astrometric parameters ($\lambda, \beta, \mu_\lambda, \mu_\beta, \pi$) and the parameters describing the stellar relative orbit with respect to the barycenter of the planetary system: period P, periastron epoch τ, eccentricity e and the 4 Thiele-Innes elements T_i, functions of semi-major axis a, inclination i, argument of periastron ω, position angle of the ascending node Ω.

The solution of the non linear system of observation equations is obtained employing an iterative linear Least Squares procedure by means of which the entire set of orbital elements can be simultaneously estimated within a well defined accuracy level. The details of this procedure are given in the following sections.

4 RESULTS

In this section we account for what is our present understanding of *GAIA*'s sensitivity to astrometric perturbations induced by Jupiter-mass planets orbiting around nearby stars. Given the present evidence of a number of extra-solar planets, we also present results on how *GAIA* would perform on a selection of three such systems.
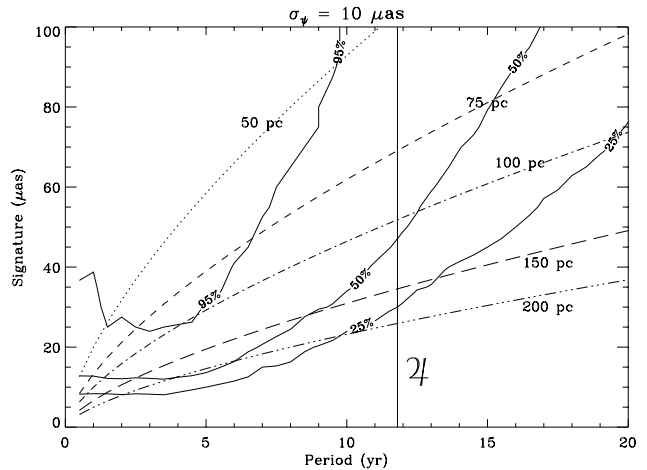
4.1 Detection probabilities

Figure 1 gives the percentage of failure of the χ^2 test on the single-star hypothesis in the case of $\sigma_\psi = 10$ μas. We note that at relatively low S/N ratios the detection probability is dominated by sampling of the orbital period. At higher S/N values orbital sampling is less critical and long period planets (up to about twice the mission duration) are detectable: as a matter of fact, when $S/N \to 10$ detection probability reaches about 100 per cent.

The dip at $P = 1$ year was somewhat expected, as both orbital motion and parallactic factor have the same period. However, the decrease is small, indicating that the coupling
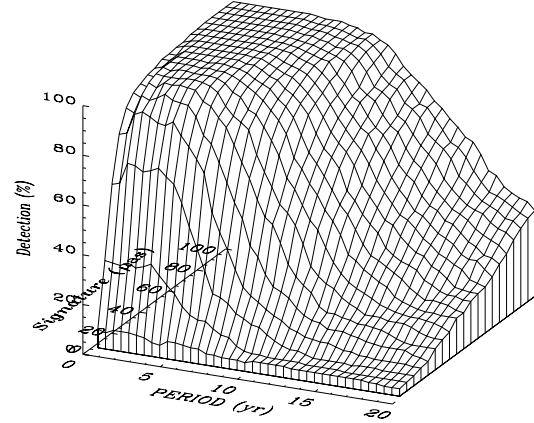
Figure 1. *Planet detection probability (percentage of failures of the χ^2 test) as function of the astrometric signature α and of the orbital period P, for $\sigma_\psi = 10$ μas. The percentage of detection of each point is based on 200 random planetary systems uniformly distributed on the sky.*

Figure 2. *Iso-probability contours (solid lines) for 25 per cent, 50 per cent and 95 per cent of detection probability, compared with Kepler's third laws (dotted/dashed lines) for systems with Jupiter-Sun masses at D=50, 75, 100, 150 and 200 pc. Jupiter-like planets (P = 11.8 yr) appear detectable, with probability $\geqslant$ 50 per cent, up to a distance of 100 pc (vertical line).*

is less critical than might have been anticipated. This is probably due to the fact that the parallactic motion has fixed phase and aspect ratio, and a relatively small mismatch in any of the orbital parameters—phase, inclination, eccentricity—is sufficient to separate the two signals.

Figure 1 also shows that the χ^2 test quickly loses its sensitivity for S/N approaching unity; thus planets for which the error in individual observations is comparable to the apparent semi-major axis are essentially undetectable with this technique.

As mentioned before, the results of Figure 1 apply to measurement errors other than the assumed $\sigma_\psi = 10$ μas, as long as the S/N value remains the same. For example, for a single observation error $\sigma_\psi = 1$ μas, the detection

probability is exactly the same as shown in Figure 1, but for amplitudes ten time smaller.

We can get important physical informations from the statistical results of Figure 1, simply changing the interpretative perspective from which we are leading the discussion. The solid lines in Figure 2 are the empirical relations, derived from Figure 1, that express the amplitude of the perturbation as a function of orbital period needed for detection probabilities of 25, 50, and 95 per cent, respectively. If the orbital period is shorter than the assumed mission lifetime of 5 years, the detection probability is about 50 per cent for $S/N \sim 1$. For longer periods, the sampling of the orbit is worse, probability drops significantly and a much higher signal is required for the planet's signature to be detected. This is in qualitative agreement with the results of Babcock (1994), who studied the *detection and convergence probability* of a complete orbital model for simulated planetary systems as observed by the mission *POINTS*. Babcock did find a slightly larger sensitivity on planet's period, manifested in an earlier turn-up and steeper slope at long periods of the 50 per cent probability curve; this most likely depends on the fact that the determination of reliable orbital elements is more challenging than detection only.

Let us now discuss the other elements of Figure 2. The overplotted dashed and dotted lines represent the signal expected for a Jupiter-mass planet and solar-mass star at various distances and orbital periods, obtained by substituting Kepler's third law in the expression for α:

$$\alpha \simeq \frac{M_p}{M_s^{2/3}} \frac{P^{2/3}}{d} \qquad (4)$$

The vertical solid line at $P = 11.8$ years indicates the locus of the actual Jupiter-Sun system at different distances. Jupiter-Sun systems appear detectable with probability $\geqslant 50$ per cent up to a distance of 100 pc, while Jupiter-mass planets with shorter periods can be detected to larger distances: to 150 pc for periods between 2.5 and 8 years. The relation can be rescaled to lower planet masses by reducing the distance of the system in proportion to the planet mass, since it is the ratio M_p/d that enters in the astrometric signature α.

Periodic photospheric activity across the disk of the parent star (e.g. star-spots cycles) can induce displacements in the position of the photocenter, thus adding astrometric signal which could be difficult to disentangle from the planet signature. However, the magnitude of such intrinsic astrometric noise appears to be at most of a few μas (Woolf & Angel 1999) for a solar-type star at a distance of 10 pc, i.e., significantly smaller than the expected single-measurement errors.

Finally, although the single-observation error significantly deteriorates with magnitude (Table 1), jovian planets around late type stars can reliably be detected at relatively large distances.

4.2   Orbital parameters estimation

The next step beyond the simple detection of candidate planets is the task of estimating the orbital parameters of each system and the mass of the unseen companion.

Our method, described in more detail below, consists
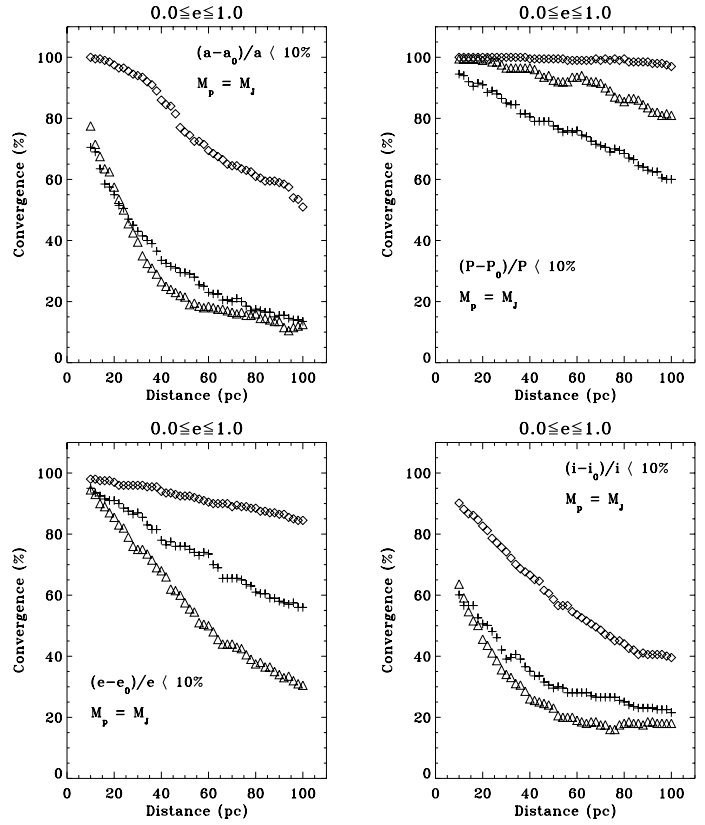
Figure 3. *Convergence probability to a 10 per cent accuracy for a, P, e, i, as function of the distance from the Sun.*

of applying an iterative non-linear least-squares fitting procedure to each of the simulated orbits; the 'known' orbital parameters are utilized as initial guesses to start the fit. Convergence of the non-linear fitting method and quality of the orbital solutions can both be significantly affected by the choice of the starting guesses. Therefore, the use of the true values of the orbital parameters to initialize the fit leaves open some important questions related to how and to what extent effective starting values, i.e., leading to successful orbital solutions, will be identified from the data as function of actual performances of the satellite, uncertainties in the error model, and properties intrinsic to planetary systems. For this, realistic global search strategies must be implemented and double-blind test campaigns conducted. Work on these issues is in progress and will be reported in the future.

Instead, this work focuses on the important goal of gauging GAIA's *ultimate* ability in measuring planets (properly, single giant planets orbiting single solar-type stars). An efficient way of achieving this is by assuming perfect knowledge of GAIA's characteristics (mainly, error model and satellite attitude) and, indeed, by using the known values of each orbital parameter as suitable initial guesses for the least-squares solutions [‡]. Then, the post-fit differences to the true values of the parameters should be a reliable measure of

---

[‡] Note that, as explained later in this section, the fitting program does not know that the initial values provided for the parameters are also their true values
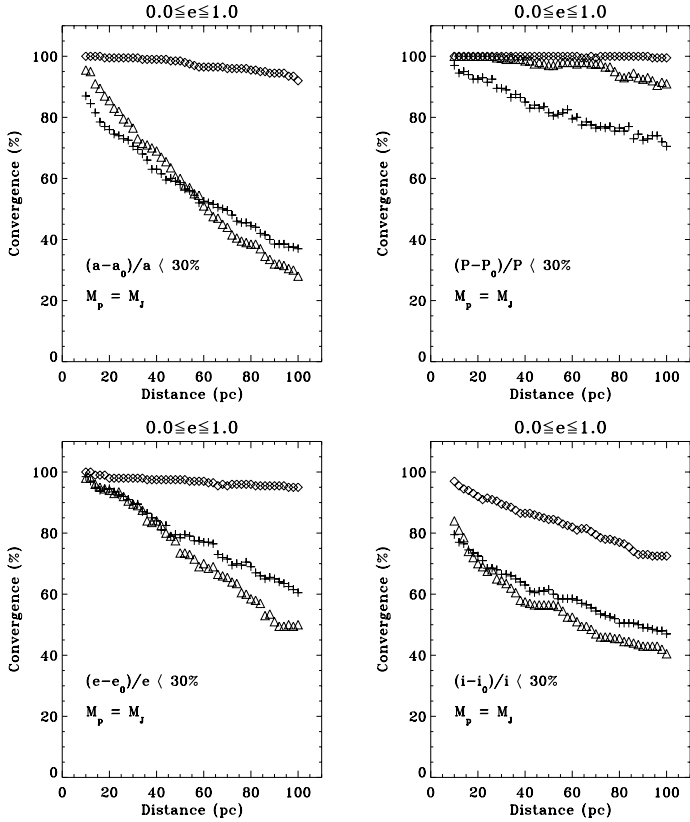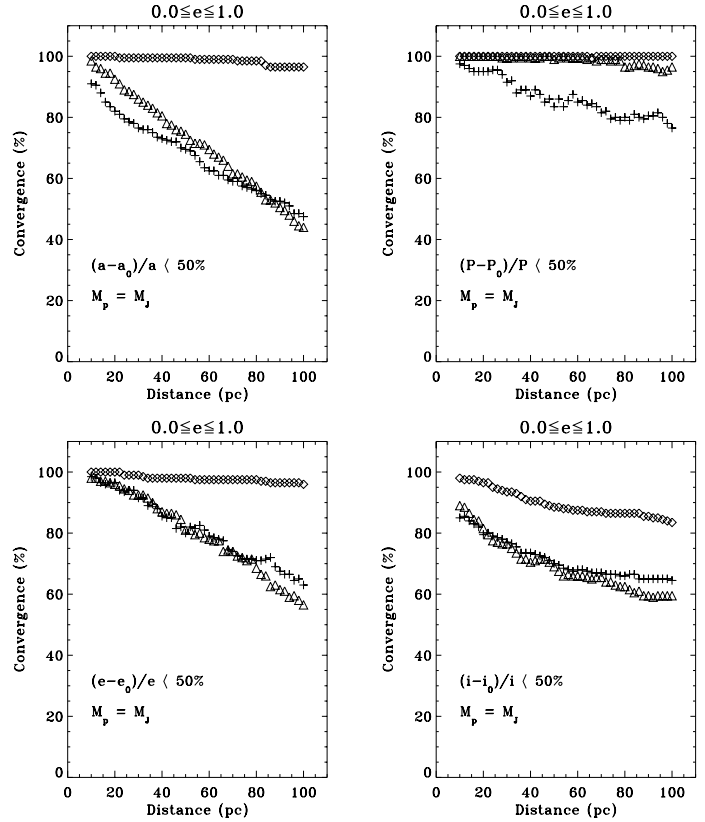
Figure 4. *Same as Figure 3, for convergence to a 30 per cent accuracy level.*

Figure 5. *Same as Figure 3, but for convergence to a 50 per cent accuracy level.*

the accuracy in orbit reconstruction that can ultimately be achieved by GAIA with the given measurement errors.

Similarly to what we did in section 4.1, we look at the accuracy of the results primarily as function of distance and orbital period. We consider systems with Sun-Jupiter masses and three values of the period: 0.5 years, to test *GAIA*'s ability to cope with poorly-sampled motion; 5 years, a near-ideal case where the orbital period is as long as the mission; and 11.8 years, the true period of the Jupiter-Sun system, which stretches *GAIA*'s ability to solve long-period orbits. For each case, we generate 200 systems randomly placed on the sky, with randomly distributed values of the other orbital parameters. These 200 systems are then placed all at the same distance, and the simulation is repeated for distance values ranging from from 10 to 100 pc.

A fit to the simulated observations is made directly at the GC level, taking into consideration a theoretical model in which *GAIA*'s unidimensional measurements are expressed as functions of the 5 astrometric parameters plus the 7 orbital elements of the keplerian orbit: for the latter we adopted a slightly linearized analytic form where semi-major axis, inclination, periastron longitude and position angle of the ascending node are combined in the four Thiele-Innes elements, while only orbital period, eccentricity and periastron epoch are left unchanged.

The first solution of the linearized system is thus found with respect to the initial guess. Then, the linearization at step k is updated with respect to the solution obtained at step $k-1$ and the process repeated until the differential cor-

rections $\delta a_{i,k}$ to each of the 12 parameters satisfy the relation: $|\delta a_{i,k}/a_{i,k-1}| < 10^{-6}$, where $i = 1, 2, \ldots, 12$ and $a_{i,k-1}$ are the parameters adjusted at the previous step. We then record what fraction of the final values for each parameter falls within a certain fractional error of the true value: this we call the "convergence probability", which is a function of the distance of the system, the period, and the desired fractional error.

We evaluate the convergence probability for the parameters which are most likely to affect the efficiency of the reconstruction of the orbit and of the mass determination, namely semimajor axis a, period P, inclination i, and eccentricity e. For each parameter, we consider fractional errors of 10, 30, and 50 per cent.

The results are shown in Figures 3 to 5. Points of different shapes correspond to different periods: triangles for 0.5 years, diamonds for 5 years, and crosses for 11.8 years. Figure 3 shows the probability of convergence within 10 per cent of the true values; Figure 4 to within 30 per cent; and Figure 5 to within 50 per cent. In each Figure, different panels correspond to different quantities.

As expected, the 5 year-period case is the best of the three. The 11.8 year period, although it corresponds to a larger signal (as the semimajor axis, and thus α, increases with period), suffers from the incomplete sampling of the orbit during the mission life-time, while the short-period case suffers from both the smaller signal amplitude and a (generally) non-optimal timing of the observations.

The periodicity of the signal is the characteristic which
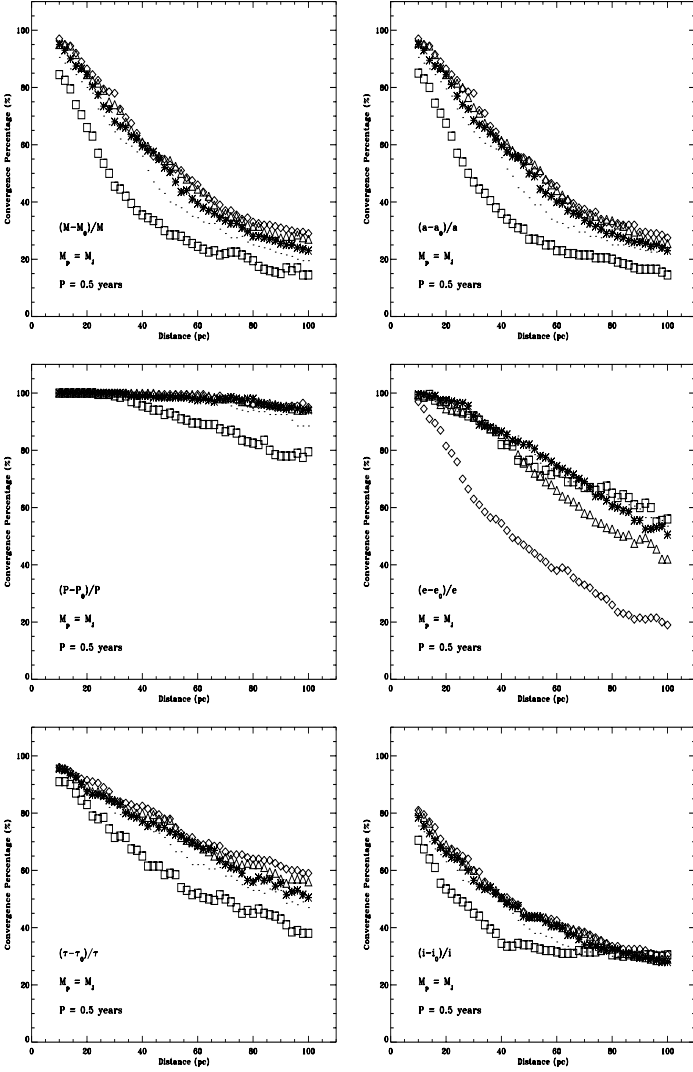
Figure 6. *The effect of eccentricity: the plots show the 20 per cent accuracy level in cases of Sun-Jupiter systems with orbital period P = 0.5 years and e set at: 0.1 (diamonds), 0.3 (triangles), 0.5 (stars), 0.7 (points), 0.9 (squares).*

Figure 7. *Same as Figure 6, for Sun-Jupiter systems with P = 5 years.*

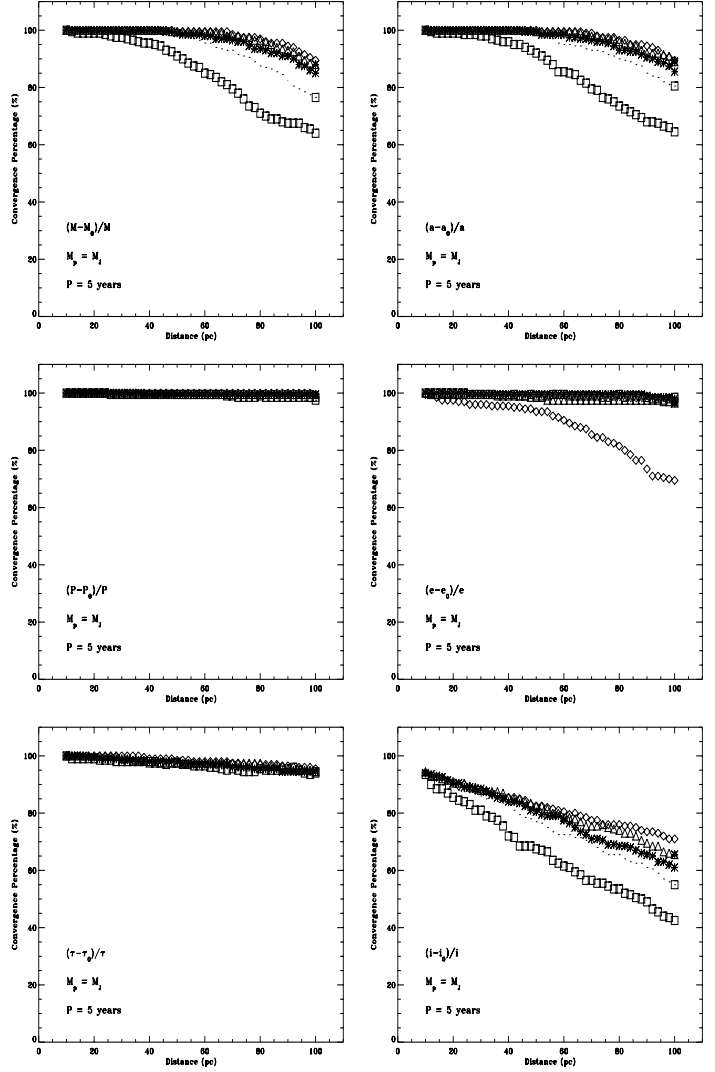can be evaluated with the best accuracy: P is the only element which is always estimated with high accuracy (better than 10 per cent) throughout the ranges covered by our simulations. We also note that the semimajor axis a and the inclination i behave similarly to each other. This may be in part a consequence of the use of the Thiele-Innes representation, since both parameters are obtained from combination of the Thiele-Innes elements.

Somewhat surprisingly, orbital eccentricity—which in the previous simulation is assumed to be distributed uniformly from 0 to 1—has a very significant effect on the quality of the estimated orbital parameters, including the mass of the planet. We illustrate this in Figures 6 through 8, where the different symbols now refer to different orbital eccentricities, and the convergence probability is given for a fixed fractional error of 20 per cent. Different figures correspond to different orbital periods. Generally, high eccentricities de-

teriorate convergence percentages for all orbital parameters. The reason is that the regularly-spaced observations of a survey satellite, such as $GAIA$, may be ill-suited to sample an orbital motion with large velocity variations, as happens for high eccentricities. The effect is especially prominent for the long-period case, $P = 11.8$ years, for such orbits will often *never* be observed during the periastron.

Our main results can thus be summarized as follows:

– For a uniform eccentricity distribution in the range $0 \leqslant e \leqslant 1$, then more than a half of all existing Jupiter-mass planets orbiting around solar-type stars with periods comparable to the mission lifetime can be detected, and their masses and orbital parameters can be estimated to an accuracy of 10 per cent up to distances of about 100 pc. From the completeness limit of the *HIPPARCOS* catalog ($V \sim 7.5 - 8$ mag) and considering spectral types no later than G5, we estimate 20 000, 65 000, and 150 000 stars to 100, 150, and 200

Figure 8. *Same as Figure 6, for Sun-Jupiter systems with P = 11.8 years.*

Figure 9. *Comparison between GAIA 50 per cent probability curve (solid line) and the minimum astrometric signature (α) induced on the parent star by presently known planetary mass objects ($0.5\,M_J \leqslant M \leqslant 11\,M_J$) in the neighborhood of our sun, as function of orbital period (log-log plot). The dahsed, dotted, and dashed-dotted lines represent the astrometric signatures induced on a solar-like star by the major solar system bodies, at increasing distance from the observer*

4.3 47 Uma, 70 Vir, and 51 Peg

We now consider more specifically how the known planetary systems fall within *GAIA*'s capabilities. *Figure 9 shows period and astrometric signature for the planets detected to date by radial velocity measurements as compared to GAIA's 50 per cent iso-probability curve.* This is the *minimum* signature, corresponding to an orbital inclination of 90°; the radial velocity method cannot generally remove the degeneracy between planetary mass and inclination. Although all systems are very close to the Sun ($d \lesssim 40$ pc), several planets have very small signatures due to their short orbital period (and thus small semi-major axis, by Kepler's third law). Some of the shortest-period objects, i.e, the 51 Peg-class planets, may prove difficult *to detect and measure* with *GAIA*. On the other hand, planets with signature $\geqslant 100\,\mu$as will be easily detected, and their orbital elements can be found with high accuracy by *GAIA*.

The considerations and results obtained in the previous sections from a statistical viewpoint are obviously preliminary to the much more difficult task of the development of self-consistent detection and orbital parameters estimation algorithms devoted to the *investigation of individual objects*, in which a more complete and realistic error model can be taken into account: to this end detailed system studies are in progress and will be presented elsewhere. It is nevertheless of interest a first glance to how well *GAIA* will behave once at work: thus, to test further *GAIA*'s capabilities of detecting periodic oscillations and signatures due to planetary companions around stars in the neighborhood of our solar

pc respectively. In this estimate the contribution from early type stars and giants is negligible. Note that these numbers increase significantly when considering spectral types earlier than K5: calculations based on current Galaxy models predict $\gtrsim 300\,000$ stars within 200 pc from the Sun (Lattanzi et al. 1999).

– For a fractional error no worse than 20 per cent, the distance limit is reduced to 50 pc for short-period and long-period orbits (0.5 and 11.8 years);

– Low-eccentricity systems are easier to detect and solve: this could indicate a potential limit in *GAIA*'s capability of reconstructing the precise behaviour of the mass function of low mass companions to solar-type stars in the neighborhood of our Sun, as to our knowledge first observational data seem to indicate than brown dwarfs are more likely to revolve around the parent stars on significantly eccentric orbits (Black 1997). On the other hand, low orbital eccentricities may be prevalent for longer periods, thus enhancing *GAIA*'s capabilities for such systems.

Figure 10. *Planetary perturbations of 47 UMa as "seen" by GAIA for an orbital inclination of 45°. The top left panel shows the path (solid line) of the star over a 5-year period. The * represent the* true *location of the star at the time of the simulated GAIA observations. The upper right panel zooms on the 0.1″ × 0.1″ region marked with a small square in the first panel. As for the two bottom graphs, they each represent a different 1-mas² enlargement of the top right panel. Again, the solid line represents the true (simulated) path of the parent star of the system. A single-star fit for 47 UMa produces the dotted path with crosses marking the calculated positions at the same observing times as before. The dashed line shows the recomputed positions after fitting the observations with a 10-parameter model (five astrometric parameters plus the four Thiele-Innes elements and the orbital period)*

system, we have concentrated our attention on the results obtained with radial velocity techniques, for what concerns three of *the star-planet systems known to date*: 47 UMa, 70 Vir and 51 Peg. All these stars are nearby and very similar to our Sun.

According to the spectroscopic measurements (Butler & Marcy 1996; Marcy & Butler 1996; Mayor & Queloz 1995), around these three stars orbit planetary bodies of minimum mass, respectively, $\sim$2.46 M_J, $\sim$6.50 M_J, and $\sim$0.5 M_J, with orbital periods of about 3 years, 4 months, 4 days. This translates in the following astrometric signatures:

$$\alpha \ (47 \ \mathrm{UMa}) \geqslant 361.88 \ \mu\mathrm{as}$$

$$\alpha \ (70 \ \mathrm{Vir}) \geqslant 167.93 \ \mu\mathrm{as}$$

$$\alpha \ (51 \ \mathrm{Peg}) \geqslant 1.66 \ \mu\mathrm{as}$$

Because of its extremely short period, the astrometric

perturbation in the case of the 51 Peg system is so small that reliable estimates of its astrometric orbit with *GAIA* will be highly difficult. On the other hand, the detection of the signatures induced on 47 UMa and 70 Vir will be extremely easy for a *GAIA*-like satellite.

We have generated 100 simulated planetary systems on the celestial sphere, respectively identical to 47 UMa and 70 Vir, assuming perfectly circular orbits and stellar masses $M = M_\odot$. The unknown orbital inclination was chosen to be $i = 45°$.

First of all, we applied the χ^2 test to the simulated observational data, with a conservative single-observation error $\sigma_\psi = 10 \ \mu$as. The detection probabilities derived are, as expected, always about 100 per cent, given the signal-to-noise ratio to be always in the regime $S/N \gg 1$.

In order to obtain a visual indication of the quality of the reconstruction, we then compared the apparent motion

Table 2. *Results of fitting GAIA observations of 47 UMa: the true orbital period simulated is $P_{\text{true}} = 2.98$ yr, the star's parallax is $\pi_{\text{true}} = 71.03$ mas. The estimated values are averages over 200 simulations per orbital inclination bin. The RMS errors are derived from direct comparison to the true values.*

i	a_{true} (μas)	a_{fit} (μas)	P_{fit} (years)	π_{fit} (mas)	$M_{\text{p,true}}$ (M_J)	$M_{\text{p,fit}}$ (M_J)
20°	1058.08	1060.92 ± 15.15	2.951 ± 0.125	71.0377 ± 0.0026	7.19	7.27 ± 0.24
30°	723.77	725.56 ± 14.45	2.956 ± 0.142	71.0377 ± 0.0029	4.92	4.97 ± 0.19
40°	562.99	565.62 ± 14.97	2.955 ± 0.119	71.0381 ± 0.0027	3.83	3.87 ± 0.15
50°	472.41	470.75 ± 14.82	2.958 ± 0.158	71.0377 ± 0.0030	3.21	3.22 ± 0.15
60°	417.87	419.63 ± 17.07	2.959 ± 0.179	71.0372 ± 0.0028	2.84	2.87 ± 0.16
70°	385.11	384.36 ± 14.48	2.973 ± 0.112	71.0378 ± 0.0026	2.62	2.62 ± 0.12
80°	367.47	367.93 ± 16.38	2.962 ± 0.157	71.0381 ± 0.0025	2.50	2.51 ± 0.14
90°	361.88	362.64 ± 15.17	2.930 ± 0.159	71.0377 ± 0.0023	2.46	2.50 ± 0.14

Table 3. *Results of fitting GAIA observations of 70 Vir: the true orbital period simulated is $P_{\text{true}} = 0.32$ yr, the star's parallax is $\pi_{\text{true}} = 55.22$ mas.*

i	a_{true} (μas)	a_{fit} (μas)	P_{fit} (years)	π_{fit} (mas)	$M_{\text{p,true}}$ (M_J)	$M_{\text{p,fit}}$ (M_J)
10°	967.05	974.56 ± 15.83	0.3198 ± 0.0015	55.2216 ± 0.0033	37.43	37.73 ± 0.62
20°	490.98	495.70 ± 15.54	0.3199 ± 0.0016	55.2211 ± 0.0027	19.00	19.19 ± 0.60
30°	335.85	339.64 ± 14.36	0.3201 ± 0.0021	55.2208 ± 0.0030	13.00	13.14 ± 0.56
40°	261.25	265.61 ± 15.37	0.3201 ± 0.0023	55.2215 ± 0.0030	10.11	10.28 ± 0.60
50°	219.21	218.48 ± 15.39	0.3198 ± 0.0023	55.2209 ± 0.0030	8.49	8.46 ± 0.60
60°	193.91	195.89 ± 17.03	0.3199 ± 0.0029	55.2205 ± 0.0028	7.51	7.58 ± 0.66
70°	178.70	181.71 ± 14.71	0.3198 ± 0.0032	55.2215 ± 0.0025	6.92	7.03 ± 0.57
80°	170.52	172.00 ± 14.23	0.3197 ± 0.0030	55.2211 ± 0.0026	6.60	6.66 ± 0.55
90°	167.93	169.69 ± 14.31	0.3198 ± 0.0042	55.2210 ± 0.0029	6.50	6.57 ± 0.56

of the star with the motion obtained with a single star fit and that obtained by a fit with the fitted parameters for the planet. Figure 10 shows the differences in 47 UMa's path on the sphere, when calculated starting from: a) the true values of μ_λ, μ_β, π, adopted in the simulation (asterisks, solid line); b) the values of μ_λ, μ_β, π, obtained after fitting the observations with a single star model (crosses, dotted line); and c) the values of μ_λ, μ_β, π and of the orbital parameters derived after fitting the observations with a 10 parameter model reproducing the standard motion plus the Keplerian circular motion induced on the observed star by the presence of the planet (diamonds, dashed line).

The annual proper motion of 47 UMa is very large, compared to the magnitude of the astrometric signature produced by the gravitational influence of its planetary companion: in ecliptic coordinates, $\mu_\lambda = -0.283$ arcsec/year, $\mu_\beta = 0.152$ arcsec/year, while $\alpha \sim 0.5$ mas for an orbital inclination of 45°. The top left panel shows the full range of motion of 47 UMa over five years; the looping motion is the parallactic eclipse, and the effect of the planet is essentially undetectable on this scale. In order to see the difference in the residuals, we zoom first on region A marked by a small square in the top left panel, then we identify in the upper right panel two 1-mas² regions (B and C), representing each a 1000x enlargement of a small fraction of the motion (bottom panels). The true and reconstructed motions are very close, consistent with the 10μas single-measurement error of the observations used to derive the orbital parameters,

while on this scale the orbit obtained with the single-star assumptions (dotted) is clearly very different from the actual motion.

Third, we derive the uncertainties in the fitted values of the important physical parameters of the two systems, and especially the companion masses. We derive the mass from the fitted orbital parameters via the mass function:

$$\frac{M_p^3}{(M_s + M_p)^2} = \frac{a_s^3}{\pi^3} \frac{1}{P^2} \tag{5}$$

where again M_p and M_s are the planetary and stellar masses in solar masses, π the parallax, P the orbital period in years, and a_s the semi-major axis of the parent star, expressed in arcsec.

Assuming $M_p \ll M_s$, we obtain:

$$M_p \simeq \left(\frac{a_s^3}{\pi^3} \frac{M_s^2}{P^2} \right)^{1/3} \tag{6}$$

Fitting the simulated observations with a 10 parameter model we can derive estimates of π and P directly, while a_s can be obtained as a combination of the approximated four Thiele-Innes elements. Provided that one gets informations about the mass of the primary, for example thanks to spectroscopy, it is possible to calculate M_p.

In our case we have, for simplicity, supposed to know M_{47UMa} and M_{70Vir} to be exactly equal to $M_\odot$.

Tables 2 and 3 show the approximated values of M_p in the two cases, starting from the estimated values of P, π and

a_s obtained during the fit, as function of orbital inclination. The Tables stop at $i = 20°$ for 47 UMa and $i = 10°$ for 70 Vir, taking into consideration the upper limits on their masses found by Perryman et al (1996) using *HIPPARCOS* data. The *HIPPARCOS* measurements, as a matter of fact, agreed with the stars to be single, as no evident signature greater than the nominal error ($\sim$1 mas) was revealed. This implies the following upper limits: $M_p \leqslant 7\ M_J$, for 47 UMa, $M_p \leqslant 38\ M_J$, for 70 Vir, which again means, considering the results obtained spectroscopically, choosing a minimum orbital inclination as in the tables. In both cases, it is clearly evident the high accuracy with which the relevant orbital parameters and the planet's mass are recovered: thanks to the fact that $S/N \gg 1$, the fit to *GAIA*'s simulated observations of 47 UMa and 70 Vir is very satisfactory; the RMS errors between fitted and nominal values of the various parameters are always well within 10 per cent.

Such results confirm that *GAIA* could reveal itself a very powerful instrument to investigate many of the known candidate planetary systems, with the exception of very short-period systems, such as 51 Peg: provided the signal-to-noise ratio is sufficiently high and the period not too short, our simulations show that such systems will be easily detected, and their orbital parameters accurately determined by *GAIA*, at least if such systems are effectively simple, as the first spectroscopic measurements would suggest. In case the signatures produced cannot be interpreted as due to the presence of only one planet, this would introduce many interpretative complications in the signals observed: for planetary systems resembling our own, detection should be little affected and residuals analysis might reveal hints of the influence of the outer planets (α for a Saturn-like companion is $\sim 60\ \mu$as at 10 pc but its period is ~ 6 times the mission lifetime). However, reliable orbital fitting would probably be restricted to the main component. On the other hand, multiple orbital fitting to good accuracy should be possible for systems composed of giant planets of comparable mass, orbiting with periods within the interval $\sim$0.5-5 yr, and yielding astrometric S/N $\gtrsim 10$, like it would be the case for the two outermost planets of the recently discovered system υ And (Butler et al. 1999).

The capability of detecting and measuring multiple planets with *GAIA* will become matter of future simulations and system studies.

5   SUMMARY AND CONCLUSIONS

In this work we have given the first quantitative evaluation of the detectability horizon of single extra-solar giant planets around single normal stars in the neighborhood of our solar system for the global astrometry mission *GAIA*. Complete simulations, comprehensive of observations of star-planet systems and successive statistical analysis of the simulated data, have yielded the following results:

a) it will be possible to detect more than 50 per cent of all *Jupiter-like* planets (orbital period $P = 11.8$ years) orbiting solar-type stars within 100 pc; *Jupiter-size* planets, with shorter orbital periods, will be detectable up to 200 pc, with similar probabilities;

b) for *true Sun-Jupiter systems* it will be possible to determine the full set of orbital parameters and to derive accurate

estimates of the masses up to distances of order of 50 pc, value which doubles if we consider the range of periods in the vicinity of the mission lifetime;

c) simulated observations of a selection of the actually known extra-solar planets, discovered by means of spectroscopic measurements, provide a meaningful estimate of the uncertainty with which masses and orbital elements can be determined for the known star-planet systems and for a substantial fraction of those that will be found within the context of such a global astrometry mission. Although preliminary, our results indicate that these systems will be easy to discover and their orbital parameters will be accurately determined with *GAIA*, except very short-period systems such as 51 Peg.

Hence, our results indicate that: 1) *GAIA* would monitor all of the hundreds of thousand F-G-K stars (i.e., whose masses are within a factor ~ 1.5 that of the Sun) up to a distance of ~ 200 pc from the Sun, in search for astrometric signatures due to the presence of giant planets ($M \simeq M_J$) with orbital periods up to Jupiter's; 2) a significant fraction of the detected planets would have the main orbital parameters (semi-major axis, period, eccentricity, inclination) measured to better than 30 per cent accuracy.

Therefore, the *GAIA* survey would uniquely complement the expectations from other ongoing and planned spectroscopic and astrometric planet searches, both from ground and in space, thus helping with the creation of the fundamental testing ground on which to measure the validity of actual theoretical models of formation and evolution. *GAIA*'s discovery potential might have significant impact on our knowledge of the distribution laws of the most relevant orbital parameters, and it would contribute to determine the frequency of planetary systems themselves in the solar neighborhood and, by extrapolation, in the whole Galaxy. A vast all-sky astrometric survey would help understand peculiar characteristics of these systems, e.g., whether giant planets lying in the outer regions are common: such planetary scenarios may be worth further investigation, as, according to present theoretical models, this could indicate presence of low mass planets in the inner regions, possibly in the parent stars' habitable zones. The monitoring of hundreds of thousands stars directly implies the chance to investigate objects belonging to a wide range of spectral types, thus providing the important observational material (Boss 1998) to decide whether giant planets are more likely to form by means of gravitational instability in disks (once they are found more often around young stars (Kuiper 1951; Cameron 1978; Bodenheimer et al. 1980)), or by means of accretion of planetesimals (once they are found more often around old stars (Pollack 1984; Lissauer 1987; Pollack et al. 1996)). The high precision global astrometric measurements will estimate the inclination i of the orbital planes for the majority of the presently known planetary systems and for a large fraction of those that will be eventually discovered: it will then be possible to provide unambiguous mass estimations of such dark companions, reducing significantly the uncertainty on the mass range in the transition region from brown dwarfs to giant planets.

ACKNOWLEDGMENTS

REFERENCES

Babcock R. W., 1994, TM94-18, CfA Technical Memorandum

Black D. C., 1997, ApJL, 490, L171

Boden A., Unwin S., Shao M., 1997, Proc. of *HIPPARCOS*: Venice '97, ESA SP-402, Ed. Battrick B., Estec, p. 789

Bodenheimer P., Grossman A. S., DeCampli W. M., Marcy G., Pollack J. B., 1980, Icarus, 41, 293

Bodenheimer P., Hubickyj O., Lissauer J., 1999, Icarus in press 1980, Icarus, 41, 293

Boss A. P., 1998, Nature, 393, 141

Butler R. P., Marcy G. W., 1996, ApJL, 464, L153

Butler R. P., et al. 1999, ApJ submitted

Cameron A. G. W., 1978, Moon Planets, 18, 5

Casertano S, et al., 1995, in Future Possibilities for Astrometry in Space, Eds. Perryman M. A. C. & van Leeuwen F., ESA SP-379

Cochran W. D., Hatzes A. P., 1994, Ap & SS, 212, 281

Cochran W. D., Hatzes A. P. Marcy G. W., Butler R. P., 1996, ApJ, 483, 457

Colavita, M. M., et al., 1998, SPIE, 3350-31, 776

Colavita, M. M., et al., 1999, APJ, 510, 505

Duquennoy A., Mayor M., 1991, A & A, 248, 485

Gai M., Lattanzi M. G., Casertano S., Guarnieri M. D., 1995, in Future Possibilities for Astrometry in Space, Eds. Perryman M. A. C. & van Leeuwen F., ESA SP-379

Gai, M. et al., 1997, Proc. of *HIPPARCOS*: Venice '97, ESA SP-402, Ed. Battrick B., Estec, p. 789

Gai, M. et al., 1998, PASP, 110, 848

Galligani I., Lattanzi M. G., Bucciarelli B., Tommasini T., Bernacca P. L., 1989, ESA SP-1111, Vol. III, p. 141

Gatewood G. D., 1987, AJ, 94, 213

Gürsel Y., 1993, in Proc. SPIE 1947, Space-borne Interferometry, Ed. Reasenberg R. D., p. 188

Gilmore, et al., 1998, in Proc. SPIE 3350, *Astronomical Interferometry*, Ed.s Reasenberg R. D. and Shao M. (astro-ph/9805180)

Kuiper G. P., 1951, Proc. Natl. Acad. Sci. U.S.A., 37, 1;

Latham, D.W. et al., 1989, Nature, 339, 38

Lattanzi M. G., et al., 1997, in Proc. 3d Internat. Conf. on Space Optics, ed. CNES(Toulouse), Session 2, Lecture 1

Lattanzi M. G., Sozzetti A., Spagna A., 1999, invited review at VLT Opening Symposium, Ed. F. Paresce (Springer Verlag), to be published

Lin D., Bodenheimer P., Richardson D., 1996, Nature, 380, 606

Lindegren L., 1995, in IAU Coll. 48, Eds. Prochazka F. V. & Tucker R. H., p. 197

Lindegren L., Perryman M. A. C., 1995, in Future Possibilities for Astrometry in Space, Eds. Perryman M. A. C. & van Leeuwen F., ESA-RGO Workshop, SP-379

Lindegren L., Perryman M. A. C., 1996, A & AS, 116, 579-595

Lissauer J. J., 1987, Icarus, 69, 249

Loiseau, S., Shaklan, S., 1996, A & AS, 117, 167

Marcy G. W., Butler R. P., 1992, PASP, 104, 270

Marcy G. W., Butler R. P., 1996, ApJL, 464, L147

Marcy G. W., Butler R. P., 1998, ARA & A, 36, 57

Marcy G., Cochran W. D., Mayor, M., 1999, in Protostars and Planets IV, Ed. V. Mannings, A. P. Boss & S. S. Russell (Tucson: University of Arizona Press), in press

Mariotti J. M., et al., 1998, SPIE 3350-33, 800

Mayor M., Queloz D., 1995, Nature, 378, 355

Mazeh T., Latham D. W., Stefanik R. P., 1996, ApJ, 466, 415

Murray N., Hansen B., Holman M., Tremaine S., 1998, Science, 279,69

Noecker M. C., 1995, in Proc. SPIE 2477, Space-borne Interferometry II

Noecker M. C., Phillips J. D., Babcock R. W., Reasenberg R. D., 1993, in Proc. SPIE 1947, Space-borne Interferometry, Ed. Reasenberg R. D., p. 174

Noyes R. W., Jha S., Korzennik S. G., Krockenberger M., Nisenson P., 1997, ApJL, 483, 111

Oppenheimer B. R., Kulkarni S. R., in *Protostars and Planets IV*, ed. V. Mannings, A. P. Boss & S. S. Russell (Tucson: University of Arizona Press), in press

Perryman M. A. C. et al., 1996, A & A, 310, L21

Pollack J. B., 1984, Annu. Rev. Astron. Astrophys., 22, 389

Pollack J. B. et al., 1996, Icarus, 124, 62

Pravdo, S. H., Shaklan, S. B., 1996, ApJ, 465, 264

Reasenberg R. D., Babcock R. W., Murison M. A., Noecker M. C., Phillips J. D., Schumaker B. L., 1995, in Proc. SPIE 2477, Space-borne Interferometry II

Trilling D., Benz W., Guillot T., Lunine J. I., Hubbard W. B., and Burrows A., 1998, ApJ, 500, 428

Unwin S., 1999, Proc. of Bioastronomy 99: A new era in Bioastronomy, to be published

Woolf N., Angel R., ARA& A, 36, 507